ADVANCED ENGINEERING MATERIALS
www.aem-journal.com

Check for updates

The Sluggish Diffusion of Cations in CeO_2 Probed through Molecular Dynamics and Metadynamics Simulations

Sylvia Körfer, Alexander Bonkowski, Joe Kler, Peter Hatton, Blas Pedro Uberuaga, and Roger A. De Souza*

Cation diffusion in fluorite-structured CeO_2, though far slower than anion diffusion, is an important, high-temperature process because it governs diverse fabrication and degradation phenomena. Herein, cation diffusion is studied by means of classical molecular dynamics and metadynamics simulations. Three different mechanisms are examined: migration involving an isolated cerium vacancy, migration involving a cerium vacancy in a defect associate with an oxygen vacancy, and migration involving a cation divacancy. For each mechanism, defect diffusion coefficients are calculated as a function of temperature, from which the respective activation enthalpy of defect migration is obtained. Through comparisons with experimental cation diffusion data (specifically, of the absolute magnitude of the cation diffusivity as well as its activation enthalpy), it is concluded that cation diffusion takes place predominantly neither by isolated vacancies nor by cation vacancy–oxygen vacancy associates but by cation divacancies.

1. Introduction

In fast oxide-ion conductors, such as fluorite-structured ceria (CeO_2), the cations are comparatively immobile, providing a stable framework within which the oxide ions can rapidly migrate. Cation transport, though sluggish, cannot be ignored, however, as it plays a central role in a variety of important phenomena: synthesis,[1–4] grain growth,[5–7] sintering,[8–10] conditioning,[11,12] creep,[13,14] interdiffusion,[15–19] kinetic demixing,[20,21] dopant segregation[17,22–25] and accumulation at extended defects,[26,27] and the precipitation of second phases.[28,29] For some phenomena (e.g., sintering), an acceleration of this sluggish process is desirable, in order to reduce the energy needed in the high-temperature production step; whereas for other phenomena (e.g., kinetic demixing), a retardation is sought (at much lower temperatures but for much longer times), in order to prolong the material's operational lifetime. Our understanding of cation transport in oxide-ion conductors lags far behind our understanding of anion transport, however. This is partly due to the relative rates of ion transport, the higher rates of anion diffusion making it far easier to determine the corresponding diffusion coefficients. But it is also partly due to the problem of interpretation.

The measured diffusion coefficient of a component in a crystal (e.g., Ce in CeO_2) can be expressed as the product of two defect quantities: the diffusion coefficient of the defects responsible for diffusion, D_{def}, and the site fraction of these defects, n_{def} (ignoring correlation factors and assuming $n_{\text{def}} \ll 1$)

$$D = D_{\text{def}} n_{\text{def}} \tag{1}$$

For cation diffusion in oxide-ion conductors, neither of the two defect quantities is easily accessible from experiment (primarily because cation defects are minority species[30]). Consequently, there is no unambiguous way to divide an experimental D value into a D_{def} value and an n_{def} value. This is the problem of interpretation.

As this problem affects, of course, D data obtained as a function of temperature, it also affects the temperature dependence of D, that is, the activation enthalpy of diffusion, ΔH_D. This quantity can be written, if D_{def} and n_{def} in Equation (1) are expressed as Boltzmann factors, as the sum of two enthalpies, $\Delta H_{\text{mig,def}}$, the activation enthalpy of defect migration, and $\Delta H_{\text{gen,def}}$, the enthalpy of defect generation

$$\Delta H_D = \Delta H_{\text{mig,def}} + \Delta H_{\text{gen,def}} \tag{2}$$

Of course, these two defect enthalpies are not easily accessible from experiment, and hence, there is no unambiguous way to divide an experimental ΔH_D value into $\Delta H_{\text{mig,def}}$ and $\Delta H_{\text{gen,def}}$. The defect enthalpies can be obtained, however, from atomistic simulations, but as we will see for CeO_2, despite the

S. Körfer, A. Bonkowski, J. Kler, R. A. De Souza
Institute of Physical Chemistry
RWTH Aachen University
Landoltweg 2, 52056 Aachen, Germany
E-mail: koerfer@pc.rwth-aachen.de

P. Hatton, B. P. Uberuaga
Materials Science and Technology Division
Los Alamos National Laboratory
Los Alamos, NM 87545, USA

The ORCID identification number(s) for the author(s) of this article can be found under https://doi.org/10.1002/adem.202201788.

© 2023 The Authors. Advanced Engineering Materials published by Wiley-VCH GmbH. This is an open access article under the terms of the Creative Commons Attribution-NonCommercial-NoDerivs License, which permits use and distribution in any medium, provided the original work is properly cited, the use is non-commercial and no modifications or adaptations are made.

DOI: 10.1002/adem.202201788

availability of predicted values, the problem with interpretation remains. A detailed understanding of cation diffusion in this material is, therefore, still missing.

Leaving to one side experimental diffusion data[31–35] for CeO_2-based solid solutions (e.g., $Ce_{0.8}Gd_{0.2}O_{1.9}$), for which defect–defect interactions complicate interpretation, we focus on the study by Beschnitt et al.[36] of Hf and Zr in weakly (0.5%) Gd-doped CeO_2. Both impurity species were found to exhibit similar cation diffusion coefficients at various temperatures, and thus, similar activation enthalpies of cation diffusion, $\Delta H_{D,Zr} = (5.5 \pm 0.4)$ eV and $\Delta H_{D,Hf} = (5.3 \pm 0.3)$ eV. Such data serve as close representatives for Ce tracer diffusion coefficients because Zr and Hf are isovalent substitutes for Ce in CeO_2 and exhibit similar, though smaller, ionic radii.

In comparison, theoretical studies of cation migration by a vacancy mechanism yield values of $\Delta H_{mig,v}$ in the range of 4.0–5.3 eV,[37–40] a result that suggests $\Delta H_{gen,v}$ is close to zero, i.e., no change in cation-vacancy concentration with temperature. The problem is that predicted equilibrium cation-vacancy concentrations increase strongly with temperature, being characterized by $\Delta H_{gen,v} > 4$ eV (according to defect chemical modeling with defect formation enthalpies and entropies from density-functional theory [DFT] calculations[41–43]). Consequently, the predicted activation enthalpy of cation diffusion (for equilibrium conditions) is $\Delta H_D > 8.4$ eV, and thus far higher than the values of ≈5.4 eV obtained experimentally under equilibrium conditions.[39] Predicted values of ΔH_D for interstitial and interstitialcy mechanisms show even larger discrepancies.

By basing such comparisons only on activation enthalpies, as only these quantities were easily amenable to simulation, one neglects the additional information provided by the absolute magnitude of the diffusion coefficient. This study aims to remedy the situation by calculating with various atomistic simulation techniques cation defect diffusion coefficients as a function of temperature, in order to compare the absolute magnitude of the cation diffusion coefficient as well as its activation enthalpy with experimental data. We focus on vacancy mechanisms for cation diffusion, given that cation vacancies are predicted to be present in far higher concentration than cation interstitials,[39] but as will be seen, it will be necessary to examine not only the simple migration mechanism but also more complex mechanisms involving point-defect associates.

2. Computational Details

All calculations in this study used established classical simulation methods,[44] based on the Born model of solids, in which the ions of the crystal lattice are treated as classical particles with nominal charge Z. The interaction of ions i and j as a function of their separation r_{ij} is described through a long-range Coulombic potential and a short-range Buckingham potential

$$V_{ij}(r_{ij}) = \left(\frac{Z_i Z_j}{4\pi\varepsilon_0 r_{ij}}\right) + A_{ij}\exp\left(-\frac{r_{ij}}{\rho_{ij}}\right) - \frac{C_{ij}}{r_{ij}^6} \quad (3)$$

with empirically determined parameters, A_{ij}, ρ_{ij}, and C_{ij}. In our simulations we employed the parameter set derived by Gotte et al.[45] All simulations in this study were performed with the software package Lammps (Large-scale Atomic/Molecular Massively Parallel Simulator).[46] In addition, we used the COLVARS library[47] implemented in Lammps for our metadynamics calculations.

2.1. NEB Calculations

Simulation cells of dimensions $6a \times 6a \times 6a$, with a being the lattice parameter of cubic ceria Ce_4O_8, were employed for the Climbing-Image Nudged-Elastic-Band (CI-NEB) calculations.[48] Depending on the migration mechanism examined, between 9 and 23 intermediate images were used.

2.2. MD Simulations

Given the high barriers reported for cation migration in CeO_2, very few cation jumps are expected to occur in molecular dynamics (MD) simulations of nanosecond duration, even at very high temperatures. In order to improve the jump statistics in MD simulations, one can increase the number of point defects present in the simulation cell, although large defect concentrations may mean that defect–defect interactions become important. One can also improve the jump statistics by increasing the size of simulation cell (at constant defect concentration), but this must be balanced against much higher computational expense. In order to obtain good jump statistics, but to keep the site fraction of cation vacancies below 1%, we performed MD simulations with supercells of dimensions $14a \times 14a \times 14a$, containing 32 928 ions, from which either 55, 56, or 100 cations were removed. The charge of the missing cations was compensated by decreasing the charge of all oxygen ions slightly.

The classical equations of motion were solved with the velocity Verlet algorithm,[49,50] with a time step of 1 fs. All simulations were performed within the isothermal–isobaric (NpT) ensemble, at temperature T and at pressure $p = 0$ GPa. A Nosé–Hoover thermostat (barostat) was employed with damping parameter of 0.2 fs (20 fs). Initially, the system was equilibrated for 50 ps to ensure that the volume and energy of the system were constant. Subsequently, a production run was performed for either 1 or 2 ns, in which the mean squared displacements of the cerium cations, $\langle r_{Ce}^2 \rangle$, were monitored. Analyzing the data with the standard relation

$$D_{Ce} = \frac{1}{6}\left(\frac{\partial \langle r_{Ce}^2 \rangle}{\partial t}\right)_T \quad (4)$$

yielded the cerium diffusion coefficient (ignoring correlation factors). As the site fraction of vacancies was known (as the number of removed cations was known), the cerium-vacancy diffusion coefficient can be obtained from Equation (1).

2.3. Metadynamics

In those cases, for which optimal simulation cells (relatively large dimensions, run for relatively long simulation times [≈2 ns] and containing many point defects) failed to provide reliable diffusion coefficients, we employed metadynamics simulations to accelerate the ion jump rate. In a metadynamics simulation, Gaussian bias potentials are imposed additively in a stepwise

© 2023 The Authors. Advanced Engineering Materials published by Wiley-VCH GmbH

15272648, 0, Downloaded from https://onlinelibrary.wiley.com/doi/10.1002/adem.202201788 by Rwth Aachen Hochschulbibliothe, Wiley Online Library on [06/06/2023]. See the Terms and Conditions (https://onlinelibrary.wiley.com/terms-and-conditions) on Wiley Online Library for rules of use; OA articles are governed by the applicable Creative Commons License

manner on the system in order to force an ion to overcome a free energy barrier and jump to an adjacent vacancy.[51–56]

According to the time-correlation-function approach of Yamamoto's rate theory[57] and Chandler's generalized approach,[58] the crossing of the free energy barrier at ξ* can be described from classical transition state theory, as

$$\Gamma = \frac{\left\langle |\dot{\xi}| \right\rangle_{\xi(0)=\xi^*}}{2} P(\xi^i) \exp\left(-\frac{\Delta G^{\ddagger}_{\mathrm{mig,v}}}{k_{\mathrm{B}} T}\right) \tag{5}$$

where $\left\langle |\dot{\xi}| \right\rangle_{\xi(0)=\xi^*}$ is the ensemble average of the velocity observable, $\left\langle |\dot{\xi}| \right\rangle$, when the system is held in ξ* at the initial point $t = 0$ (it is divided by 2 to include only successful crossings); $P(\xi^i)$ is the probability density of finding the system in the initial configuration, ξ^i ; and $\Delta G^{\ddagger}_{\mathrm{mig,v}}$ denotes the activation Gibbs energy of migration.[54,59] One important feature is the selection of one or more collective variables (CVs), ξ(*r*), that describe the migration path. In our simulations, spatial coordinates in the Cartesian coordinate system were employed.

The three terms in Equation (5) were calculated by applying appropriate MD sampling techniques.[60] $\Delta G^{\ddagger}_{\mathrm{mig,v}}$ was computed by introducing bias potentials stepwise in metadynamics simulations. The probability density at the initial state of the system $P(\xi^i)$ was obtained from straightforward MD simulations, in which the histogram of the ion's trajectory along ξ is examined. And the third term, $\left\langle |\dot{\xi}| \right\rangle_{\xi(0)=\xi^*}$, was calculated by constrained MD simulations, in which the migrating ion was first confined at the top of the barrier, and then allowed to move, so that $|\dot{\xi}|$ is obtained. To get $\left\langle |\dot{\xi}| \right\rangle_{\xi(0)=\xi^*}$, a large number of simulation runs are performed.[54,60]

Having obtained the jump rate Γ, one can calculate the defect diffusion coefficient according to

$$D_{\mathrm{v}} = \frac{Z}{6} d_{\mathrm{v}}^2 \Gamma \tag{6}$$

where Z is the number of nearest jump neighbors and d_{v} is the jump distance. In the case of cation migration by a vacancy mechanism along the ⟨110⟩ direction, $Z = 12$ and $d_{\mathrm{v}}(T) = [a_0 + T\alpha a_0]/\sqrt{2}$, where a_0 corresponds to the lattice parameter of cubic CeO_2 at $T = 0$ K and α to the linear thermal expansion coefficient.[61]

For metadynamics calculations we used supercells of size $6a \times 6a \times 6a$ with 2592 ions, to which a single cation vacancy or a single defect associate was introduced. Here, too, the simulations were carried out within the *NpT* ensemble. The equilibration time of the system was again 50 ps and the time step Δt was set to 1 fs for the isolated cation vacancy mechanism, and 0.5 fs for the associate mechanisms. By reducing Δt, we avoided instabilities in the numerical integration scheme, which otherwise led to problems or collapse of the simulation at longer simulation times and larger time steps. The times of the metadynamics simulation runs were (3–5) ns. Gaussian bias potentials of height ω (0.005 or 0.01 eV) and width σ (0.4 Å) were added to the system at a frequency of $1/\delta t$ ($\delta t = 100$ fs).

3. Results

The main aim of this study is to achieve a deeper understanding of cation transport in CeO_2 by comparing theoretical predictions with experimental data, taking into account not only the activation enthalpy but also the absolute magnitude of cation diffusion. As experimental data we take, in the absence of Ce tracer diffusion data, the diffusion coefficients of Hf and Zr in CeO_2 obtained for $1400 \leq T/\mathrm{K} \leq 1600$ in air by Beschnitt et al.[36]

$$D_{\mathrm{Hf}}(T) = 6.7 \times \exp\left(-\frac{(5.3 \pm 0.3)\,\mathrm{eV}}{k_{\mathrm{B}} T}\right) \mathrm{cm^2\,s^{-1}} \tag{7}$$

$$D_{\mathrm{Zr}}(T) = 25.1 \times \exp\left(-\frac{(5.5 \pm 0.4)\,\mathrm{eV}}{k_{\mathrm{B}} T}\right) \mathrm{cm^2\,s^{-1}} \tag{8}$$

As these cations will presumably migrate in CeO_2 by the same mechanism as Ce does, this is a reasonable approach. From Equation (7) and (8), we obtain cation diffusion coefficients, e.g., at $T = 1500$ K, of $D_{\mathrm{Hf}} = 1.0 \times 10^{-17}\,\mathrm{cm^2\,s^{-1}}$ and $D_{\mathrm{Zr}} = 8.3 \times 10^{-18}\,\mathrm{cm^2\,s^{-1}}$. That is, the activation enthalpy of cation diffusion is ≈5.4 eV and the cation diffusion coefficient at $T = 1500$ K is of the order of $10^{-17}\,\mathrm{cm^2\,s^{-1}}$.

3.1. Migration by Cerium Monovacancies

The lowest energy jump of a Ce cation into an adjacent vacancy takes place, according to various simulations,[39] along the ⟨110⟩ direction of CeO_2, as indicated in **Figure 1**a. Our NEB calculations for this migration mechanism are shown in Figure 1b: they yield an activation energy of $\Delta E^{\ddagger}_{\mathrm{mig,v}} = 5.18$ eV. The calculations also confirm previous results[39] that the path is not straight but curved between initial and final configuration (not shown).

The first attempt to obtain cation tracer diffusion coefficients for this mechanism employed MD simulations. As shown in **Figure 2**, the mean-squared displacement of the cerium ions, $\left\langle r^2_{\mathrm{Ce}} \right\rangle$, obtained from such simulations was constant at all temperatures investigated. Thus, according to Equation (4), no diffusion had occurred, and indeed, examination of the simulation cells indicated that no successful cation jumps took place during the simulations. The increase in the constant value of $\left\langle r^2_{\mathrm{Ce}} \right\rangle$ with increasing temperature reflects the increased amplitude of the Ce ion vibrations. The absence of diffusion is not entirely unexpected, given the extremely high activation barrier of 5.18 eV predicted with NEB calculations. In other words, the MD simulations of cation diffusion by a monovacancy mechanism were unsuccessful for the accessible simulation times.

In a second attempt to obtain tracer diffusion coefficients, we turned to metadynamics simulations (see Section 2.3). In **Figure 3**a we show, as an example, the Gibbs energy surface $G(\xi)$ for the migration of a Ce cation into a neighboring vacancy at $T = 1700$ K. In Figure 3b, in which the free energy surface is shown as a heatmap, the curved nature of the two equivalent migration paths, from initial to final configuration, via two equivalent saddle-point configurations are evident, as already found in the NEB calculations. Results obtained as a function of temperature are plotted in **Figure 4**a. Extrapolating these data linearly down to 0 K (i.e., assuming a constant activation entropy of

© 2023 The Authors. Advanced Engineering Materials published by Wiley-VCH GmbH

15272648, 0, Downloaded from https://onlinelibrary.wiley.com/doi/10.1002/adem.202201788 by Rwth Aachen Hochschulbibliothe, Wiley Online Library on [06/06/2023]. See the Terms and Conditions (https://onlinelibrary.wiley.com/terms-and-conditions) on Wiley Online Library for rules of use; OA articles are governed by the applicable Creative Commons License

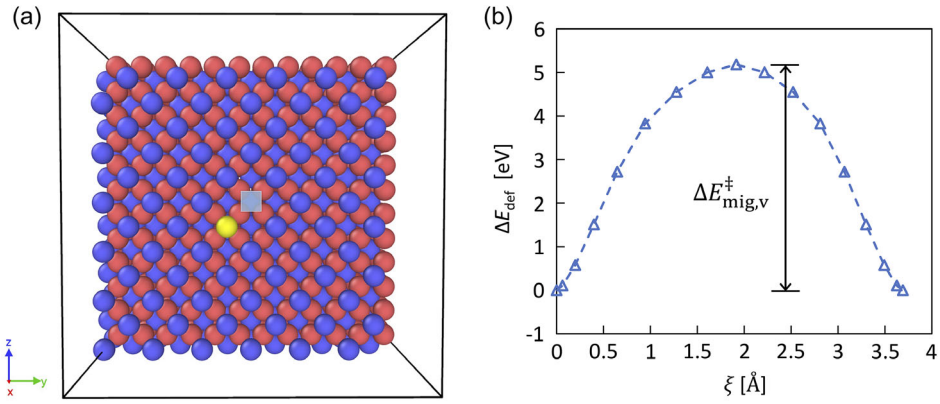


Figure 1. a) Schematic illustration of the mechanism of an isolated Ce vacancy in ceria (Ce cations: blue spheres; O anions: red spheres; migrating Ce cation: yellow sphere; isolated Ce vacancy: light blue square) (visualized by the Open Visualization Tool [OVITO][67]). b) NEB energy profile for the cerium ion migration into an isolated cerium vacancy along its respective pathway ξ.

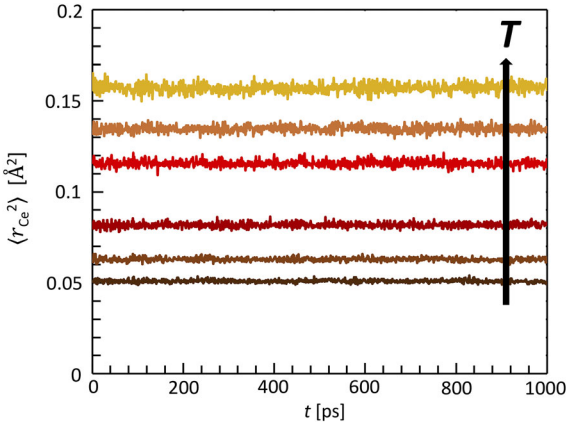


Figure 2. Mean square displacements of Ce cations, $\langle r_{Ce}^2 \rangle$, versus time t for different temperatures, as obtained from MD simulations of cells containing isolated cation vacancies (data are shown for temperatures T [K]: 1000, 1200, 1500, 2000, 2250, 2500).

migration), we find $\Delta G^{\ddagger}_{mig,v}(0\,K) = \Delta H^{\ddagger}_{mig,v} = (5.45 \pm 0.36)$ eV. This value agrees well with the value of $\Delta E^{\ddagger}_{mig,v}$ determined from NEB simulations.

In addition to $\Delta G^{\ddagger}_{mig,v}$, we need $P(\xi^i)$ und $\left\langle |\dot{\xi}| \right\rangle_{\xi(0)=\xi^*}$ in order to calculate the cation-vacancy jump rate according to Equation (5). The values obtained for these two parameters are shown in Figure 4b,c. The probability density $P(\xi^i)$ decreases continuously with increasing temperature (Figure 4b), which is due to the increase in the vibrational amplitude of the (migrating) Ce cation on its lattice site. For the conditional ensemble average of the velocity observable at the saddle point of the system, $\left\langle |\dot{\xi}| \right\rangle_{\xi(0)=\xi^*}$, an increase in velocity with an increasing temperature is seen (Figure 4c), which can be simply attributed to the higher temperature, and thus, a higher kinetic energy.

Calculating with these data (Figure 4a–c) values of D_v for cerium-vacancy migration according to Equation (6), we obtain the data shown in Figure 4d. The effective

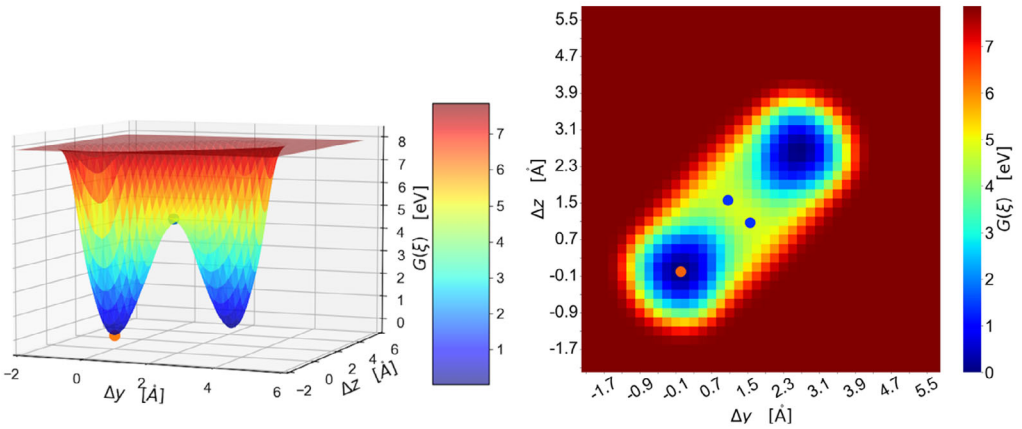


Figure 3. The Gibbs energy surface $G(\xi)$ for the migration of a Ce cation by a monovacancy mechanism along the Δy and Δz collective coordinates as computed by metadynamics simulations at $T = 1700$ K. The starting point, ξ^i, of the migration pathway is marked with an orange dot; the two equivalent saddle point configurations, ξ*, are marked with blue dots.

© 2023 The Authors. Advanced Engineering Materials published by Wiley-VCH GmbH

15272648, 0, Downloaded from https://onlinelibrary.wiley.com/doi/10.1002/adem.202201788 by Rwth Aachen Hochschulbibliothe, Wiley Online Library on [06/06/2023]. See the Terms and Conditions (https://onlinelibrary.wiley.com/terms-and-conditions) on Wiley Online Library for rules of use; OA articles are governed by the applicable Creative Commons License

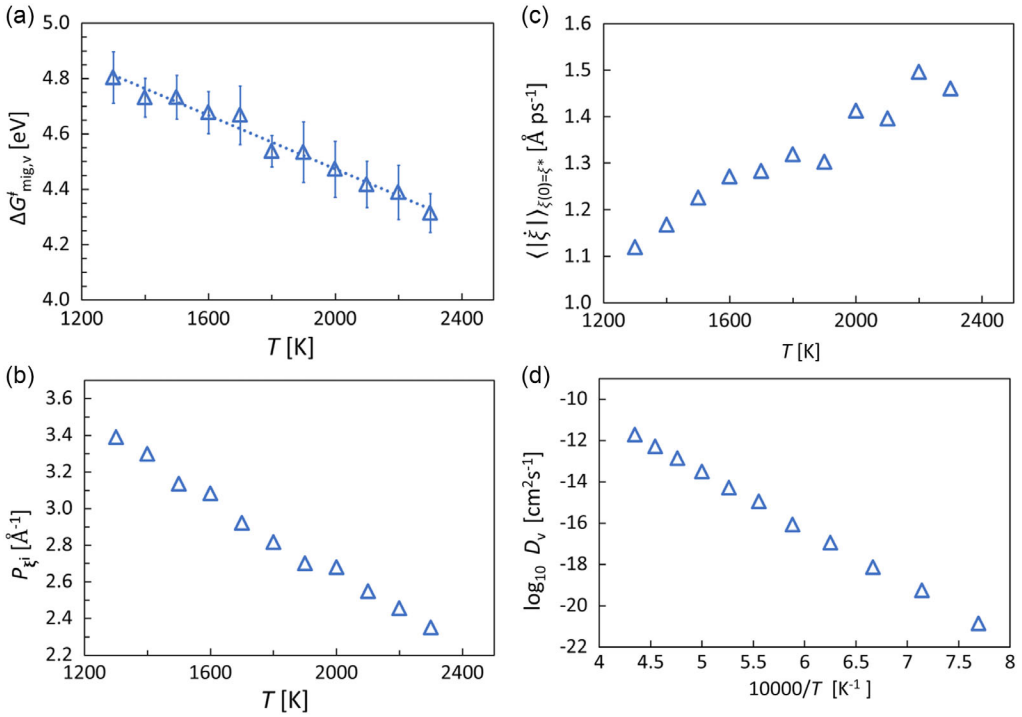


Figure 4. Cerium-vacancy diffusion in CeO_2 by the migration of a cerium monovacancy. a) Gibbs activation energy of cerium-vacancy migration, $\Delta G^{\ddagger}_{\mathrm{mig,v}}$, as computed by metadynamics simulations as a function of temperature T; b) probability density at the initial system configuration ξ^i, $P(\xi^i)$, as obtained from MD simulations; c) conditional ensemble average of the collective coordinate velocity $\dot{\xi}$, $\left\langle |\dot{\xi}| \right\rangle_{\xi(0)=\xi^*}$, as calculated by constrained MD simulations; d) cation-vacancy diffusion coefficients D_v (symbol size indicates the error bars) as a function of inverse temperature.

activation enthalpy of migration, determined from $\Delta H^{\ddagger\mathrm{eff}}_{\mathrm{mig,v}} = -k_B[\mathrm{d}\ \ln D_v(T)/\mathrm{d}\ T^{-1}]$, is $\Delta H^{\ddagger\mathrm{eff}}_{\mathrm{mig,v}} = (5.4 \pm 0.4)$ eV. This value agrees very well with the experimental value of $\Delta H_D = 5.4$ eV obtained experimentally by Beschnitt et al.[36] (Equation (7), (8), but this good agreement is misleading. Comparing the absolute magnitude of the cation diffusion coefficients at $T = 1500$ K, we find an unphysical result. In order to obtain $D \approx 10^{-17}\ \mathrm{cm^2\,s^{-1}}$ from the predicted vacancy diffusivity of $D_v = 7.3 \times 10^{-19}\ \mathrm{cm^2\,s^{-1}}$ by means of Equation (1), we require $n_v \geq 1$. That is, we require more vacancies to be present than sites to accommodate them. This obviously makes no physical sense, and hence we must conclude that, according to these simulations, cation diffusion in ceria cannot occur predominantly by the migration of isolated cation vacancies.

3.2. Migration by Cation Vacancy–Anion Vacancy Associates

Given that oxygen vacancies are one of the predominant point defects in acceptor-doped CeO_2, one could surmise that a defect associate of a cerium vacancy with an oxygen vacancy is responsible for cation diffusion (**Figure 5**a). NEB calculations for this mechanism yielded an activation barrier of 5.49 eV (Figure 5b). The migration path is no longer curved in the yz plane, but linear; in addition, the path does not remain with this plane, but is displaced in the direction of the missing oxygen ion. As the activation barrier is of the same order of magnitude as that for the simple vacancy mechanism (see Section 3.1), we assumed that MD simulations would similarly provide no cation diffusion coefficients. We therefore continued our studies with metadynamics simulations. The results are shown in **Figure 6** and **7**.

Figure 6 shows the Gibbs energy surface $G(\xi)$ for the migration mechanism. The migration path is linear along the yz-direction and slightly curved in the direction of the O-vacancy, confirming the NEB results (Figure 5).

Figure 7 summarizes the results of the simulations for this migration mechanism, including defect diffusion coefficients D_v calculated according to Equation (6), with the same value for the jump distance $d_v(T)$ as before but with $Z = 3$. From the Arrhenius plot, we obtain an effective activation enthalpy of $\Delta H^{\ddagger\mathrm{eff}}_{\mathrm{mig,v}} = (4.9 \pm 0.6)$ eV.

In comparison with the monovacancy mechanism, this associate mechanism has a slightly lower activation enthalpy (4.90 vs 5.41 eV) and slightly higher defect diffusion coefficients. Nevertheless, the site fraction of vacancies, according to Equation (1), required to reproduce the experimental cation diffusion data of Beschnitt et al.[36] (at $T = 1500$ K, see Section 3) is still unphysical with $n_v \geq 1$. Thus, this mechanism can also be rejected as the dominant mechanism of cation diffusion in CeO_2.

3.3. Migration by a Divacancy Mechanism

As it was not possible to describe the experimental data of Beschnitt et al.[36] with the two previous mechanisms, we consider a third possibility: a divacancy mechanism, i.e., two

© 2023 The Authors. Advanced Engineering Materials published by Wiley-VCH GmbH

15272648, 0, Downloaded from https://onlinelibrary.wiley.com/doi/10.1002/adem.202201788 by Rwth Aachen Hochschulbibliothe, Wiley Online Library on [06/06/2023]. See the Terms and Conditions (https://onlinelibrary.wiley.com/terms-and-conditions) on Wiley Online Library for rules of use; OA articles are governed by the applicable Creative Commons License

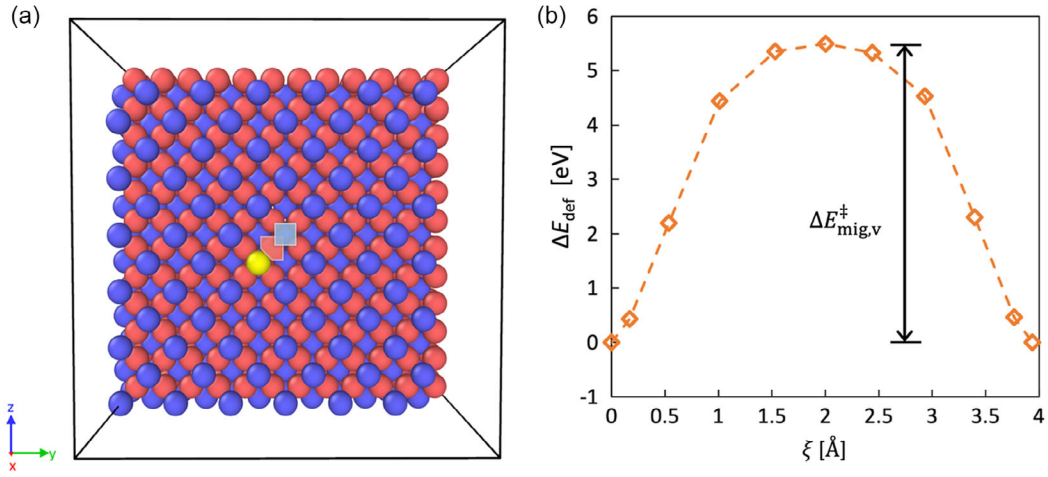


Figure 5. a) Schematic illustration of the mechanism of cerium-vacancy migration with an adjacent oxygen vacancy (Ce cations: blue spheres; O anions: red spheres; migrating Ce cation: yellow sphere; isolated Ce vacancy: light blue square; adjacent O vacancy: light red square) (visualized by OVITO[67]). b) NEB energy profile for the Ce migration into a cerium vacancy with an adjacent oxygen vacancy along its respective pathway ξ.

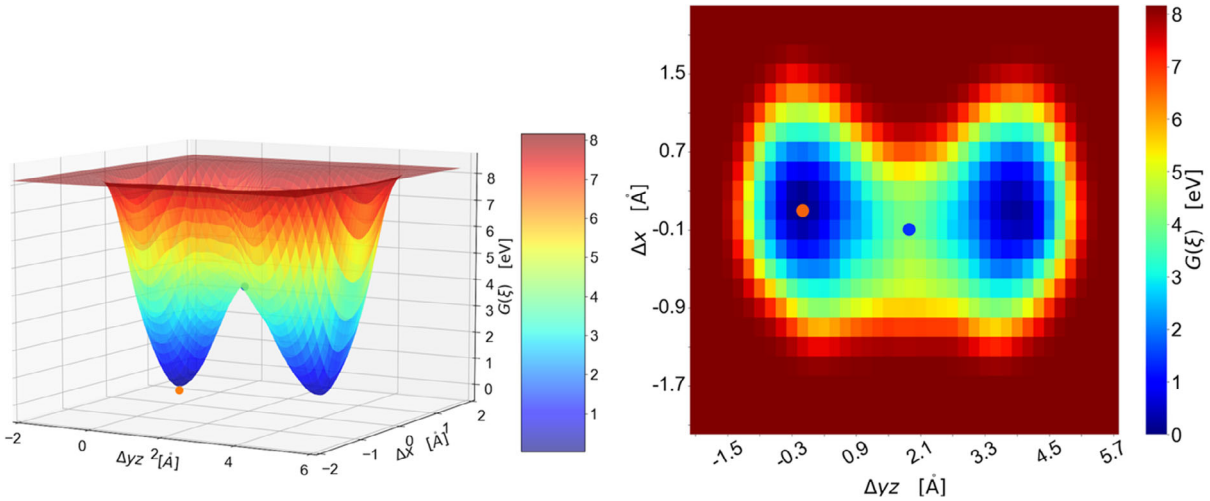


Figure 6. Illustration of the averaged Gibbs energy surfaces $G(\xi)$ for the v'''_{Ce} migration with an adjacent $v^{\cdot\cdot}_{O}$ along the Δy and Δz collective coordinates as computed by metadynamics simulations at $T = 1700$ K. The starting point, ξ^i, of the migration pathway is marked with an orange dot and the top of the migration barrier, ξ*, with a blue dot. On the right side the 2D mapping of the surface shows that the adjacent O-vacancy causes a bending in the migration pathway of the Ce cation.

adjacent cation vacancies. In a DFT study of cation diffusion in fluorite-structured UO_2, Andersson et al.[62] found that a divacancy mechanism had a substantially lower migration barrier for uranium migration (2.6 eV) than the monovacancy mechanism (4.5 eV).

The arrangement of two neighboring cation vacancies in CeO_2 is shown in **Figure 8**a. One vacancy is situated in the uppermost plane, and the second in the plane beneath the intermediate plane of oxygen ions. The two cation vacancies are geometrically equivalent, so that the marked cation can theoretically jump into either vacancy. NEB calculations revealed an energy profile (Figure 8b) with two energetically identical maxima and a local minimum; in addition, the jumping cation was predicted to take a complex path (not shown), one not constrained to a single plane. The activation barrier for the jump from the initial site over the first maximum is 1.85 eV. This value is substantially lower than the activation barrier of 5.18 eV calculated for the monovacancy migration mechanism (see Section 3.1), and hence, in good qualitative agreement with the results of Andersson et al.[62] for uranium migration in UO_2.

Metadynamics simulations did not yield any diffusion coefficient in this case because the simulations either did not converge or were unstable. We attribute these difficulties to this mechanism's complex migration path, which, because it was not confined to a single plane, necessitated the use of three, rather than two, collective variables. However, given the much lower activation energy obtained in the NEB calculations for this mechanism, cation diffusion coefficients could be obtained directly from

© 2023 The Authors. Advanced Engineering Materials published by Wiley-VCH GmbH

15272648, 0, Downloaded from https://onlinelibrary.wiley.com/doi/10.1002/adem.202201788 by Rwth Aachen Hochschulbibliothe, Wiley Online Library on [06/06/2023]. See the Terms and Conditions (https://onlinelibrary.wiley.com/terms-and-conditions) on Wiley Online Library for rules of use; OA articles are governed by the applicable Creative Commons License

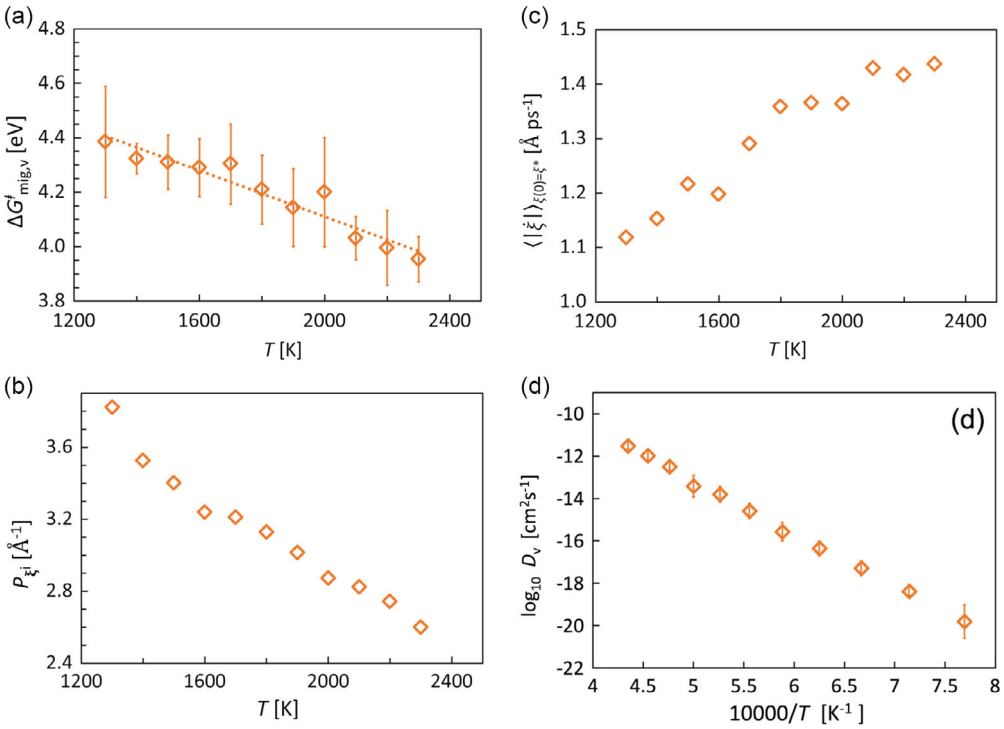


Figure 7. Cerium-vacancy diffusion in CeO_2 by the migration of a cerium vacancy–oxygen vacancy associates. a) Gibbs activation energy of cerium-vacancy migration, $\Delta G^{\ddagger}_{mig,v}$, as computed by metadynamics simulations as a function of temperature T; b) probability density at the initial system configuration ξ^i, $P(\xi^i)$, as obtained from MD simulations; c) conditional ensemble average of the collective coordinate velocity $\dot{\xi}$, $\left\langle |\dot{\xi}| \right\rangle_{\xi(0)\xi=^*}$, as calculated by constrained MD simulations; d) cation-vacancy diffusion coefficients D_v (symbol size indicates the error bars) as a function of inverse temperature.

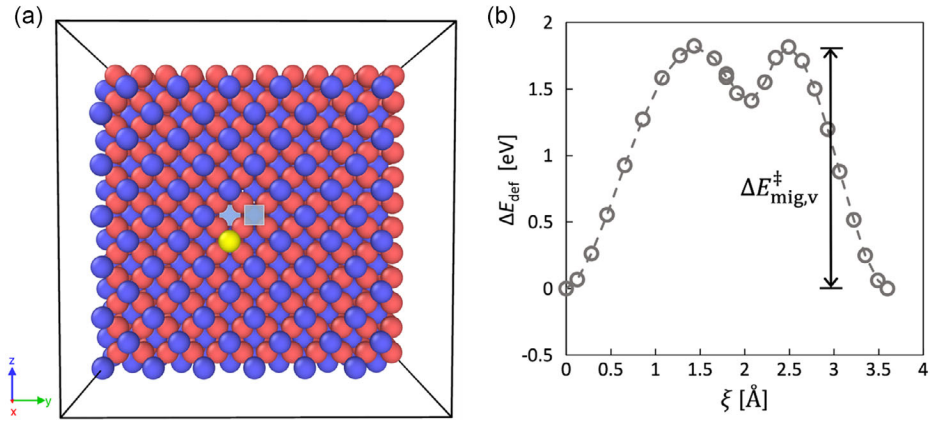


Figure 8. a) Schematic illustration of the Ce divacancy mechanism (Ce cations: blue spheres; O anions: red spheres; migrating Ce cation: yellow sphere; isolated Ce vacancies: light blue squares) (visualized by OVITO[67]). b) NEB energy profile for the Ce divacancy mechanism. Migration of a Ce cation along its respective pathway ξ.

standard MD simulations. At temperatures in the range $2600 \leq T/\mathrm{K} \leq 3000$, the mean square displacements of the Ce cations, $\left\langle r^2_{Ce} \right\rangle$, was observed to increase significantly with simulation time t, as shown in **Figure 9** (cf., Figure 2 for the mono-vacancy case). As the jump rates were still rather low, we performed at each temperature ten MD simulations with different initial conditions, to improve the statistics. From each $\left\langle r^2_{Ce} \right\rangle(t)$ curve, we calculated using Equation (4) a cerium diffusivity, and subsequently, using Equation (1), a cerium-vacancy diffusivity. The results are plotted in **Figure 10**.

We note two important points. First, although the simulation temperatures are rather high (higher than the experimental melting point of CeO_2), we did not observe any lattice melting in the MD simulations. The diffusion data refer, therefore, to the

© 2023 The Authors. Advanced Engineering Materials published by Wiley-VCH GmbH

15272648, 0, Downloaded from https://onlinelibrary.wiley.com/doi/10.1002/adem.202201788 by Rwth Aachen Hochschulbibliothe, Wiley Online Library on [06/06/2023]. See the Terms and Conditions (https://onlinelibrary.wiley.com/terms-and-conditions) on Wiley Online Library for rules of use; OA articles are governed by the applicable Creative Commons License

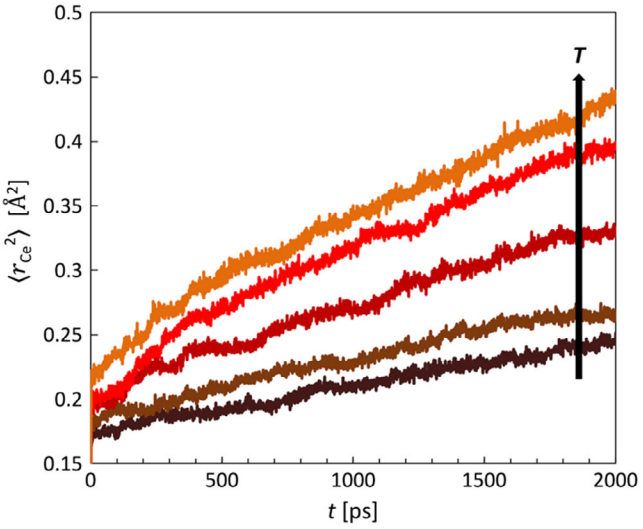


Figure 9. Mean square displacements of Ce cations, $\langle r_{Ce}^2 \rangle$, versus time t for different temperatures, as obtained from MD simulations of cells containing cation divacancies (data are shown for temperatures T [K]: 2600, 2700, 2800, 2900, 3000). Only one dataset is shown at each temperature (from a possible ten datasets).

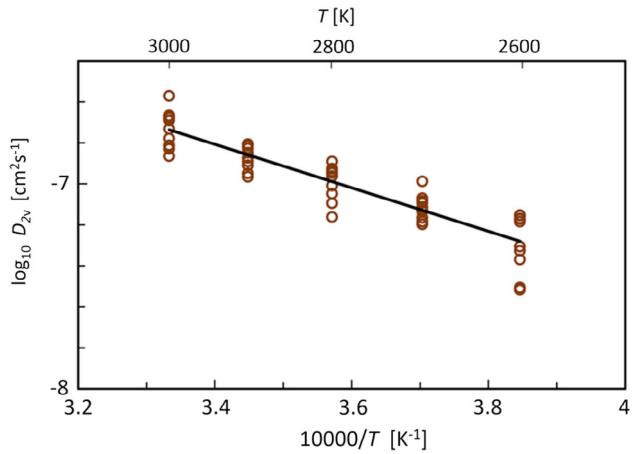


Figure 10. Divacancy diffusion coefficients, D_{2v}, as a function of inverse temperature, as obtained from MD simulations.

crystalline lattice rather than a liquid phase. Second, almost all divacancies remain bound during the MD simulations. At the highest temperature examined, a few divacancies dissociated, leaving monovacancies in next nearest-neighbor positions. Thus, the diffusion data refer to the migration of cation divacancies.

The effective activation enthalpy of migration by a divacancy mechanism is found to be $\Delta H_{mig,2v} = (2.10 \pm 0.28)$ eV. Within the margin of error, this value is in good agreement with the result of the NEB calculations (1.85 eV). In comparison with the experimental value of ≈5.4 eV from Beschnitt et al.,[36] it is much lower, but this discrepancy is not an issue. According to Equation (2), ΔH_D can have two contributions, and hence, our MD results indicate that the enthalpy of defect generation is $\Delta H_{gen,2v} \approx (5.4 - 2.1)$ eV ≈ 3.3 eV. Furthermore, extrapolating our MD data down to $T = 1500$ K, we obtain a defect diffusivity, $D_{2v} \approx 10^{-10}$ cm^2 s^{-1}, that requires a physically reasonable value for the site fraction of defects, $n_{2v} \approx 10^{-7}$, in order to reproduce $D \approx 10^{-17}$ cm^2 s^{-1}. We conclude, therefore, that of the three mechanisms examined, only the divacancy mechanism permits a physically reasonable description of the experimental diffusion data of Beschnitt et al.[36]

Finally, in this section we calculate $\Delta H_{gen,2v}$ by an alternative route, i.e., through defect chemical modeling. We begin with the formation of cation divacancies according to (in Kröger–Vink notation[63,64])

$$v_{Ce}^{4\prime} + v_{Ce}^{4\prime} \rightleftharpoons (v_{Ce}v_{Ce})^{8\prime} \tag{9}$$

with the equilibrium constant of divacancy formation of

$$K_{dvf} = \frac{n_{2v}}{(n_v^{cat})^2} = K_{dvf}^0 \exp\left(-\frac{\Delta H_{dvf}}{k_B T}\right) \tag{10}$$

Cation monovacancies are considered to form by means of the Schottky equilibrium

$$Ce_{Ce}^{\times} + 2O_O^{\times} \rightleftharpoons v_{Ce}^{4\prime} + 2v_O^{\cdot\cdot} + CeO_2 \tag{11}$$

with equilibrium constant

$$K_{Sch} = n_v^{cat}(n_v^{an})^2 = K_{Sch}^0 \exp\left(-\frac{\Delta H_{Sch}}{k_B T}\right) \tag{12}$$

Combining Equation (10) and (12), we obtain

$$n_{2v} = K_{dvf} K_{Sch}^2 (n_v^{an})^{-4} \tag{13}$$

and thus

$$\Delta H_{gen,2v} = -k_B \frac{d \ln n_{2v}}{d(1/T)} = \Delta H_{dvf} + 2\Delta H_{Sch} + 4k_B \frac{d \ln n_v^{an}}{d(1/T)} \tag{14}$$

The last term in Equation (14) characterizes how the site fraction of oxygen vacancies varies with temperature. For the system of interest ($n_{Gd} = 0.5\%$) in air and in the temperature range examined experimentally ($1400 \leq T/K \leq 1600$), n_v^{an} is not fixed by the acceptor-dopant level, but varies because oxide reduction generates a significant amount of oxygen vacancies. A defect chemical calculation (not shown) based on a reduction free energy predicted by DFT calculations[41–43] of $(4.21 - 17.5\, k_B T)$ eV yields a value of −4.3 eV for the last term. Thus, with $\Delta H_{gen,2v} \approx 3.3$ eV, we obtain from Equation (14) that $\Delta H_{dvf} + 2\Delta H_{Sch} \approx 7.6$ eV. With the predicted[41] enthalpy of Schottky disorder, $\Delta H_{Sch} = 6.87$ eV, the enthalpy of divacancy formation would then be ≈−6 eV, which seems rather high. If the predicted value of ΔH_{Sch} is, however, an overestimation, then the magnitude of ΔH_{dvf} would also be overestimated. For example, with $\Delta H_{Sch} = 5$ eV, the formation energy of a divacancy from two monovacancies would be $\Delta H_{dvf} = -2.3$ eV, which seems far more reasonable.

© 2023 The Authors. Advanced Engineering Materials published by Wiley-VCH GmbH

15272648, 0, Downloaded from https://onlinelibrary.wiley.com/doi/10.1002/adem.202201788 by Rwth Aachen Hochschulbibliothe, Wiley Online Library on [06/06/2023]. See the Terms and Conditions (https://onlinelibrary.wiley.com/terms-and-conditions) on Wiley Online Library for rules of use; OA articles are governed by the applicable Creative Commons License

4. Discussion

In their highest charge state, cerium vacancies carry a fourfold relative charge, and hence, the formation of cation divacancies, $(v_{Ce}v_{Ce})^{8\prime}$, appears improbable, at least from the viewpoint of simple electrostatics. This is not the complete picture, though, because elastic interactions also need to be taken into account, and they may provide stabilization. Indeed, for UO_2, Andersson et al.[65] predicted $\Delta H_{dvf} = -0.3$ eV for $(v_U v_U)^{8\prime}$ from DFT calculations; this enthalpy, though small, is nevertheless negative, indicating a bound, fully charged divacancy. Another source of stabilization may be the addition of one or more oxygen vacancies. And again for UO_2, $(v_U v_U v_O)^{6\prime}$ clusters are predicted[62] to be stable, with a binding energy of -2.84 eV. Cation migration within such a cluster was only slightly higher than for migration by means of the cation divacancy without the oxygen vacancy,[62] a result that emphasizes the importance of cation divacancies in some form for low migration barriers.

Why does the divacancy mechanism have such a low activation enthalpy of migration? The available computational data are consistent with the migration barrier being governed by Coulomb interactions, and specifically repulsive interactions with other cations (cf., ref. [66] for anion migration in CeO_2). Removal of a cation adjacent to a cation vacancy thus produces a configuration in which the migration barrier is substantially lowered; adding one or more oxygen vacancies to this configuration will subsequently cause comparatively minor effects. This explanation suggests, in turn, that a cation trivacancy associate would be characterized by an even lower activation barrier. We contend, however, that a cation divacancy, with or without additional oxygen vacancies, already constitutes a rather large void in a crystal lattice, and hence that the even larger cation trivacancies are extremely unlikely to form. To determine the stability of divacancy and higher order defect associates in CeO_2, a set of careful DFT calculations is required.

On the subject of alternative mechanisms, we note that Dong et al.[38] propose that cation migration takes place by a polaron mechanism, that is, the cation prefers to migrate as Ce^{3+} rather than Ce^{4+}, on account of a lower activation barrier. This mechanism is problematic because it requires the polaron either to reside on a cation next to a cation vacancy for a period of time many orders of magnitude longer than its normal residence time at a cation (and we consider this highly unlikely), or to arrive just as the cation is about to jump (and we consider the frequency of such synchronous events to be extremely low). We performed NEB calculations of a Ce^{3+} jump into a monovacancy, and we confirmed a decrease in the migration barrier: in our case, 4.44 eV for Ce^{3+} migration versus 5.18 eV for Ce^{4+} migration (see Section 3.1). This lower barrier is, however, still much higher than the barrier we find for the divacancy mechanism (≈2 eV, Section 3.3). Consequently, according to our simulations, the polaron mechanism can be discarded as the dominant mechanism of cation migration.

Finally, we examine the process of cation-divacancy formation. Given that cation monovacancies are rather immobile, it may be that such a vacancy, once formed at a surface through Schottky disorder, does not move away because its jump rate is so low. Rather, it is only once a neighboring cation vacancy has formed that the jump rate rises by many orders of magnitude, and the divacancy can thus move away from the surface. This argument does not require the divacancy to have a negative binding energy; it would be sufficient for the migration barrier for the dissociation of the divacancy to be much higher than the divacancy migration barrier, so that the divacancy has a sufficiently long lifetime. Preliminary NEB calculations indicate a barrier for the jump away, i.e., for the dissociation step, of 4.6 eV, which is considerably higher than the ≈2 eV for the divacancy mechanism. These values are consistent with the behavior observed in the MD simulations: the vast majority of the divacancies remain bound, at least for the duration of the simulations.

5. Conclusion

In this work, we investigated cation diffusion in CeO_2 using molecular dynamics and metadynamics simulations. Our intention was to describe experimental cation diffusion data, in order to elucidate the dominant cation diffusion mechanism. To this end, we examined three migration mechanisms: by a cation monovacancy, by a defect associate of a cation vacancy with an oxygen vacancy, and by a cation divacancy. The benefit of our approach—comparing diffusivities as well as activation enthalpies—is clear. If we had only considered the activation enthalpy of diffusion, we would have concluded that the first two mechanisms are consistent with experimental data. By using the absolute value of the cation diffusivity, however, we were able to conclude that these mechanisms cannot be operative. Consequently, we find that, in some form, cation divacancies play the decisive role for cation diffusion in ceria.

Acknowledgements

The German Research Foundation (DFG) is gratefully acknowledged for funding within the framework of the priority program SPP1959 "Manipulation of Matter Controlled by Electric and Magnetic Fields: Towards Novel Synthesis and Processing Routes of Inorganic Materials" under project DE 2854/9-2. Simulations were performed with computing resources granted by RWTH Aachen University under the Project Nos. rwth0617 and rwth0809. P.H. and B.P.U. acknowledge support by the U.S. Department of Energy, Office of Science, Basic Energy Sciences, Materials Sciences and Engineering Division under grant number LANLE4BU. Los Alamos National Laboratory, an affirmative action equal opportunity employer, is managed by Triad National Security, LLC for the U.S. Department of Energy's NNSA, under contract 89233218CNA000001.

Open Access funding enabled and organized by Projekt DEAL.

Conflict of Interest

The authors declare no conflict of interest.

Data Availability Statement

The data that support the findings of this study are available from the corresponding author upon reasonable request.

© 2023 The Authors. Advanced Engineering Materials published by Wiley-VCH GmbH

15272648, 0, Downloaded from https://onlinelibrary.wiley.com/doi/10.1002/adem.202201788 by Rwth Aachen Hochschulbibliothe, Wiley Online Library on [06/06/2023]. See the Terms and Conditions (https://onlinelibrary.wiley.com/terms-and-conditions) on Wiley Online Library for rules of use; OA articles are governed by the applicable Creative Commons License

Keywords

cation diffusion, CeO_2, divacancies, mechanisms, simulations

Received: December 9, 2022
Revised: January 30, 2023
Published online:

[1] K. Eguchi, T. Setoguchi, T. Inoue, H. Arai, *Solid State Ionics* **1992**, *52*, 165.
[2] Y. Wang, T. Mori, J. G. Li, T. Ikegami, *J. Am. Ceram. Soc.* **2002**, *85*, 3105.
[3] Y. Wang, T. Mori, J. G. Li, Y. Yajima, *Sci. Technol. Adv. Mater.* **2003**, *4*, 229.
[4] S. B. Bošković, D. R. Djurović, S. P. Zec, B. Z. Matović, M. Zinkevich, F. Aldinger, *Ceram. Int.* **2008**, *34*, 2001.
[5] V. Gil, C. Moure, P. Durán, J. Tartaj, *Solid State Ionics* **2007**, *178*, 359.
[6] S. Kurajica, I. K. Munda, F. Brleković, K. Mužina, G. Dražić, J. Šipušić, M. Mihaljević, *J. Solid State Chem.* **2020**, *291*, 121600.
[7] D. D. Upadhyaya, R. Bhat, S. Ramanathan, S. K. Roy, H. Schubert, G. Petzow, *J. Eur. Ceram. Soc.* **1994**, *14*, 337.
[8] S. Sameshima, K. Higashi, Y. Hirata, in *The Korea Association of Crystal Growth: Proceedings of the Korea Association of Crystal Growth Conf.* **2000**, p. 65.
[9] S. J. Hong, A. V. Virkar, *J. Am. Ceram. Soc.* **1995**, *78*, 433.
[10] T. Mori, R. Buchanan, D. R. Ou, F. Ye, T. Kobayashi, J.-D. Kim, J. Zou, J. Drennan, *J. Solid State Electrochem.* **2008**, *12*, 841.
[11] S. M. Stewart, R. L. Borup, M. S. Wilson, A. Datye, F. H. Garzon, *ECS Trans.* **2014**, *64*, 403.
[12] M. G. Cutrufello, I. Ferino, V. Solinas, A. Primavera, A. Trovarelli, A. Auroux, C. Picciau, *Phys. Chem. Chem. Phys.* **1999**, *1*, 3369.
[13] F. Iguchi, Y. Endo, T. Ishida, K. Sato, T. Hashida and H. Yugami, in *Solid State Ion.: The Science and Technology of Ions in Motion – Proceedings of the 9th Asian Conf.*, (Eds. B. V. R. Chowdari, H.-I. Yoo, G. M. Choi, J.-H. Lee), World Scientific, Jeju Island, South Korea **2004**, 179.
[14] J. L. Routbort, K. C. Goretta, A. R. de Arellano-López, J. Wolfenstine, *Scr. Mater.* **1997**, *38*, 315.
[15] H. Xu, K. Cheng, M. Chen, L. Zhang, K. Brodersen, Y. Du, *J. Power Sources* **2019**, *441*, 227152.
[16] A. Tsoga, A. Gupta, A. Naoumidis, P. Nikolopoulos, *Acta Mater.* **2000**, *48*, 4709.
[17] Z.-P. Li, T. Mori, G. J. Auchterlonie, J. Zou, J. Drennan, *J. Solid State Chem.* **2011**, *184*, 2458.
[18] A. Tsoga, A. Gupta, A. Naoumidis, D. Skarmoutsos, P. Nikolopoulos, *Ionics* **1998**, *4*, 234.
[19] S. Uhlenbruck, T. Moskalewicz, N. Jordan, H.-J. Penkalla, H. P. Buchkremer, *Solid State Ionics* **2009**, *180*, 418.
[20] G. Petot-Ervas, C. Petot, *Ionics* **2005**, *11*, 189.
[21] M. Martin, *Solid State Ionics* **2000**, *136*, 331.
[22] Z.-P. Li, T. Mori, G. J. Auchterlonie, J. Zou, J. Drennan, *Appl. Phys. Lett.* **2011**, *98*, 093104.
[23] K. Sato, *J. Phys. Chem. C* **2015**, *119*, 5734.
[24] V. A. Sadykov, V. V. Kriventsov, E. M. Moroz, Y. V. Borchert, D. A. Zyuzin, V. P. Kol'ko, T. G. Kuznetsova, V. P. Ivanov, S. Trukhan, A. I. Boronin, E. M. Pazhetnov, N. V. Mezentseva, E. B. Burgina, J. R. H. Ross, *Solid State Phenom.* **2007**, *128*, 81.
[25] D. R. Ou, T. Mori, F. Ye, J. Zou, G. Auchterlonie, J. Drennan, *Electrochem. Solid-State Lett.* **2007**, *10*, P1, doi: 10.1149/1.2372224.
[26] D. S. Mebane, R. A. De Souza, *Energy Environ. Sci.* **2015**, *8*, 2935.
[27] X. Tong, D. S. Mebane, R. A. De Souza, *J. Am. Ceram. Soc.* **2020**, *103*, 5.
[28] H. Yahiro, T. Ohuchi, K. Eguchi, A. Hiromichi, *J. Mater. Sci.* **1988**, *23*, 1036.
[29] F. Ye, T. Mori, D. R. Ou, J. Zou, J. Drennan, *Mater. Res. Bull.* **2007**, *42*, 943.
[30] M. Mueller, K. Pingen, A. Hardtdegen, S. Aussen, A. Kindsmueller, S. Hoffmann-Eifert, R. A. De Souza, *APL Mater.* **2020**, *8*, 081104.
[31] A. Tsoga, A. Naoumidis, D. Stöver, *Solid State Ionics* **2000**, *135*, 403.
[32] Y. Sakka, Y. Oishi, K. Ando, S. Morita, *J. Am. Ceram. Soc.* **1991**, *74*, 2610.
[33] M. Izuki, M. E. Brito, K. Yamaji, H. Kishimoto, D.-H. Cho, T. Shimonosono, T. Horita, H. Yokokawa, *J. Power Sources* **2011**, *196*, 7232.
[34] N. Sakai, H. Kishimoto, K. Yamaji, T. Horita, M. E. Brito, H. Yokokawa, *J. Electrochem. Soc.* **2007**, *154*, B1331.
[35] J. A. Kilner, D. Waller, J. D. Sirman, in *Solid Oxide Fuel Cells V: Proc. of the Fifth Inter. Symp. on Solid Oxide Fuel Cells* (Eds: U. Stimming, S. C. Singhal, H. Tagawa), The Electrochemical Society, Pennington, NJ **1997**, p. 1159.
[36] S. Beschnitt, R. A. De Souza, *Solid State Ionics* **2017**, *305*, 23.
[37] A. Guglielmetti, A. Chartier, L. van Brutzel, J.-P. Crocombette, K. Yasuda, C. Meis, S. Matsumura, *Nucl. Instrum. Methods Phys. Res., Sect. A* **2008**, *266*, 5120.
[38] Y. Dong, L. Qi, A. Alvarez, J. Li, I.-W. Chen, *Acta Mater.* **2022**, *232*, 117941.
[39] S. Beschnitt, T. Zacherle, R. A. De Souza, *J. Phys. Chem. C* **2015**, *119*, 27307.
[40] H. Y. Xiao, Y. Zhang, W. J. Weber, *J. Nucl. Mater.* **2011**, *414*, 464.
[41] T. Zacherle, A. Schriever, R. A. De Souza, M. Martin, *Phys. Rev. B* **2013**, *87*, 134104.
[42] M. Martin, T. Zacherle, A. Schriever, R. A. De Souza, S. Grieshammer, *ECS Trans.* **2013**, *57*, 2405.
[43] S. Grieshammer, T. Zacherle, M. Martin, *Phys. Chem. Chem. Phys.* **2013**, *15*, 15935.
[44] C. R. A. Catlow, W. C. Mackrodt, *Lecture Notes in Physics*, Vol. *166*, Springer-Verlag, Berlin, Heidelberg, New York **1982**, p. 3.
[45] A. Gotte, D. Spångberg, K. Hermansson, M. Baudin, *Solid State Ionics* **2007**, *178*, 1421.
[46] A. P. Thompson, H. M. Aktulga, R. Berger, D. S. Bolintineanu, W. M. Brown, P. S. Crozier, P. J. in't Veld, A. Kohlmeyer, S. G. Moore, T. D. Nguyen, R. Shan, M. J. Stevens, J. Tranchida, C. Trott, S. J. Plimpton, *Comput. Phys. Commun.* **2022**, *271*, 108171.
[47] G. Fiorin, M. L. Klein, J. Hénin, *Mol. Phys.* **2013**, *111*, 3345.
[48] G. Henkelman, B. P. Uberuaga, H. Jónsson, *J. Chem. Phys.* **2000**, *113*, 9901.
[49] L. Verlet, *Phys. Rev.* **1967**, *159*, 98.
[50] W. C. Swope, H. C. Andersen, P. H. Berens, K. R. Wilson, *J. Chem. Phys.* **1982**, *76*, 637.
[51] A. Barducci, M. Bonomi, M. Parrinello, *Wiley Interdiscip. Rev.: Comput. Mol. Sci.* **2011**, *1*, 826.
[52] A. Laio, M. Parrinello, *Proc. Natl. Acad. Sci.* **2002**, *99*, 12562.
[53] A. Laio, F. L. Gervasio, *Rep. Prog. Phys.* **2008**, *71*, 126601.
[54] D. Frenkel, B. Smit, in *Understanding Molecular Simulation* (Eds: D. Frenkel, B. Smit), Academic Press, New York **2002**, Ch. 16.
[55] B. J. Berne, in *Multiple Time Scales* (Eds: J. U. Brackbill, B. I. Cohen), Academic Press, New York **1985**, Ch. 13.
[56] M. Borkovec, P. Talkner, *J. Chem. Phys.* **1990**, *92*, 5307.
[57] T. Yamamoto, *J. Chem. Phys.* **1960**, *33*, 281.
[58] D. Chandler, *J. Chem. Phys.* **1978**, *68*, 2959.
[59] J. Koettgen, P. C. Schmidt, T. Bučko, M. Martin, *Phys. Rev. B* **2018**, *97*, 024305.
[60] H. J. Heelweg, R. A. De Souza, *Phys. Rev. Mater.* **2021**, *5*, 013804.
[61] V. Grover, A. K. Tyagi, *Mater. Res. Bull.*, **2004**, *39*, 859.

© 2023 The Authors. Advanced Engineering Materials published by Wiley-VCH GmbH

15272648, 0, Downloaded from https://onlinelibrary.wiley.com/doi/10.1002/adem.202201788 by Rwth Aachen Hochschulbibliothe, Wiley Online Library on [06/06/2023]. See the Terms and Conditions (https://onlinelibrary.wiley.com/terms-and-conditions) on Wiley Online Library for rules of use; OA articles are governed by the applicable Creative Commons License

[62] D. A. Andersson, B. P. Uberuaga, P. V. Nerikar, *Phys. Rev. B* **2011**, *84*, 054105.
[63] F. Kröger, H. Vink, *Solid State Phys.* **1956**, *3*, 307.
[64] T. Norby, J. Korean. *Ceram. Soc.* **2010**, *47*, 19.
[65] D. A. Andersson, P. Garcia, X.-Y. Liu, G. Pastore, M. Tonks, P. Millett, B. Dorado, D. R. Gaston, D. Andrs, R. L. Williamson, R. C. Martineau, B. P. Uberuaga, C. R. Stanek, *J. Nucl. Mater.* **2014**, *451*, 225.
[66] A. R. Genreith-Schriever, P. Hebbeker, J. Hinterberg, T. Zacherle, R. A. De Souza, *J. Phys. Chem. C* **2015**, *119*, 28269.
[67] A. Stukowski, *Modell. Simul. Mater. Sci. Eng.* **2010**, *18*, 015012.

© 2023 The Authors. Advanced Engineering Materials published by Wiley-VCH GmbH

15272648, 0, Downloaded from https://onlinelibrary.wiley.com/doi/10.1002/adem.202201788 by Rwth Aachen Hochschulbibliothe, Wiley Online Library on [06/06/2023]. See the Terms and Conditions (https://onlinelibrary.wiley.com/terms-and-conditions) on Wiley Online Library for rules of use; OA articles are governed by the applicable Creative Commons License